ACS APPLIED MATERIALS & INTERFACES

Research Article

www.acsami.org

Thermoplastic Polyurethane:Polythiophene Nanomembranes for Biomedical and Biotechnological Applications

Maria M. Pérez-Madrigal,[†,‡] Marina I. Giannotti,[§,∥,⊥] Luis J. del Valle,[†] Lourdes Franco,[†,‡] Elaine Armelin,[†,‡] Jordi Puiggalí,[†,‡] Fausto Sanz,*[,§,∥,⊥] and Carlos Alemán*[,†,‡]

[†]Departament d'Enginyeria Química, ETSEIB, Universitat Politècnica de Catalunya, Avda. Diagonal 647, Barcelona E-08028, Spain

[‡]Center for Research in Nano-Engineering, Universitat Politècnica de Catalunya, Campus Sud, Edifici C', C/Pasqual i Vila s/n, Barcelona E-08028, Spain

[§]CIBER de Bioingeniería, Biomateriales y Nanomedicina, CIBER-BBN, Madrid, 28029, Spain

[∥]Departament de Química Física, Facultat de Química, Universitat de Barcelona, Martí i Franqués 1, Barcelona 08028, Spain

[⊥]Institut de Bioenginyeria de Catalunya, IBEC, Baldiri i Reixac 15-21, Barcelona 08028, Spain

Supporting Information

ABSTRACT: Nanomembranes have been prepared by spin-coating mixtures of a polythiophene (P3TMA) derivative and thermoplastic polyurethane (TPU) using 20:80, 40:60, and 60:40 TPU:P3TMA weight ratios. After structural, topographical, electrochemical, and thermal characterization, properties typically related with biomedical applications have been investigated: swelling, resistance to both hydrolytic and enzymatic degradation, biocompatibility, and adsorption of type I collagen, which is an extra cellular matrix protein that binds fibronectin favoring cell adhesion processes. The swelling ability and the hydrolytic and enzymatic degradability of TPU:P3TMA membranes increases with the concentration of P3TMA. Moreover, the degradation of the blends is considerably promoted by the presence of enzymes in the hydrolytic medium, TPU:P3TMA blends behaving as biodegradable materials. On the other hand, TPU:P3TMA nanomembranes behave as bioactive platforms stimulating cell adhesion and, especially, cell viability. Type I collagen adsorption largely depends on the substrate employed to support the nanomembrane, whereas it is practically independent of the chemical nature of the polymeric material used to fabricate the nanomembrane. However, detailed microscopy study of the morphology and topography of adsorbed collagen evidence the formation of different organizations, which range from fibrils to pseudoregular honeycomb networks depending on the composition of the nanomembrane that is in contact with the protein. Scaffolds made of electroactive TPU:P3TMA nanomembranes are potential candidates for tissue engineering biomedical applications.

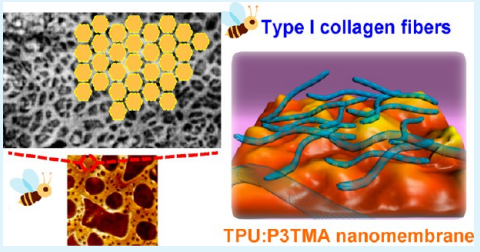

KEYWORDS: *bioactive platform, biodegradable blend, collaged adsorption, scaffolds, ultrathin films, tissue engineering*

INTRODUCTION

The design of electrically conducting devices for biomedical and biotechnological applications has become a topic of growing interest.[1] Concretely, these devices use the electromagnetic fields that regulate biological processes to interact with tissues. Intrinsic conducting polymers (ICPs) are being widely studied as suitable candidates for these biomedical devices because of both their electrical behavior and biocompatibility. Among other applications, ICPs have been used as biosensors,[2] neural electrodes,[3] biactuators,[4] drug delivery systems,[5] or tissue scaffolds.[6,7] For tissue engineering purposes, conducting scaffolds are intended to display similar features (chemical, mechanical, and topological) to those characteristic of the extracellular matrix (ECM) in native tissues, thus performing as an adequate substrate onto which cells are able to attach and communicate. Furthermore, their electrical properties can regulate cellular functions such as adhesion, migration, proliferation, and differentiation via electrical stimulation.[8]

However, ICPs exhibit brittleness and poor mechanical properties when used individually. Therefore, the blending of ICP with another polymer, generally insulating, results in flexible conducting polymer-based scaffolds. Generally, the polymeric matrix embeds the ICP moieties, thus improving the mechanical stability and processability of the final product. To obtain flexible ICP-based scaffolds that reproduce the structure and function of the ECM, several approaches have been followed by using different polymeric materials as the matrix (elastomers[9] and hydrogels[10,11]) and microfabrication technology for tailoring topographical and mechanical properties[12] and functional nanomaterials, which include nanofibers,[13] nanotubes,[5] or nanomembranes.[14]

Interestingly, research of robust ultrathin membranes made of two macroscopic dimensions and one nanodimension has

Received: April 9, 2014
Accepted: May 23, 2014
Published: May 23, 2014

   dx.doi.org/10.1021/am502150q | ACS Appl. Mater. Interfaces 2014, 6, 9719−9732

been recently brought into focus.[15] Although in the past decade several authors have reported self-supported nanomembranes made by inorganic materials (e.g., silicon, metal, nanoparticles, carbon nanotubes, and grapheme),[16−20] the number of studies based on soft materials is still relatively scarce. Recently, Kunitake and co-workers used a spin-coating method to fabricate robust and flexible nanomembranes made of a variety of cross-linked synthetic materials (e.g., inorganic-soft material hybrids, thermosetting resins, and photopolymers).[21−25] Nevertheless, the biocompatibility and elasticity of these nanomembranes were not comparable to those of basement membranes, which are amorphous sheet-like structures of fibers that underlie the epithelium and play a critical role in cell proliferation, differentiation, and migration. Furthermore, free-standing nanomembranes have been also prepared using biopolymers (e.g., polysaccharides, silk, and biodegradable polylactic acid).[26−28]

Within this context, we recently reported the fabrication of robust and flexible nanomembranes made of a mixture of poly(butylene succinate) and poly(3-thiophene methyl acetate) (P3TMA).[29,30] Hydrolytic and enzymatic degradation studies combined with cell viability assays allowed us to propose their potential application as bioactive platforms for tissue engineering. In a very recent study, Lee and co-workers[31] described the fabrication of large-area free-standing ultrathin membranes made of polydimethylsiloxane, a widely used silicon-based organic polymer with diverse biomedical applications.[32,33] These nanomembranes, which are highly pliable (i.e., easily bendable or shaped) and biocompatible, were used to analyze the mechanical properties of cellular epithelia.

Our most recent research has been focused on the fabrication and nanometric characterization of nanomembranes made of a thermoplastic polyurethane matrix (TPU) and P3TMA.[34,35] More specifically, the topological, nanomechanical, nanoconducting, and electrochemical properties of TPU:P3TMA nanomembranes, which were prepared by spin-coating the solution of the mixture (40:60 weight ratio), were characterized by atomic force microscopy (AFM), quantitative nanomechanical (QNM) AFM, conductive AFM (C-AFM), and cyclic voltammetry (CV), respectively. The surface of 40:60 TPU:P3TMA nanomembranes was described as the combination of the topographies of both individual components.[34] This resulted in a homogeneous distribution of granules throughout the surface, which were associated with the P3TMA rich phase by conductive C-AFM measurements. Both 40:60 TPU:P3TMA and P3TMA nanomembranes showed semiconductor behavior with very similar band gap energy (2.35 and 2.32 eV, respectively),[35] which was attributed to the influence of the fabrication process on the π-conjugation length and packing interactions of P3TMA chains. The current and conductivity values determined for the nanomembranes, which ranged from 0.43 to 1.85 pA and from 2.23×10^{-5} to 5.19×10^{-6} S/cm, respectively, evidenced inhomogeneity in the P3TMA-rich domains.[35] Furthermore, the voltammetric response of TPU:P3TMA and P3TMA nanomembranes was found to be similar in terms of ability to store charge and electrochemical stability.[35]

In this work studies have been conducted to further explore TPU:P3TMA nanomembranes behavior as biointerfaces. In an effort to relate the influence of the composition for tailoring purposes, the structural, electrochemical, and thermal properties of samples prepared considering 20:80, 40:60, and 60:40 weight ratios have been compared. After this, properties associated with potential biomedical applications of TPU:P3TMA blends (i.e., swelling, degradation, biocompatibility, and ability to adsorb extra cellular matrix proteins) were examined.

METHODS

Materials and Synthesis of P3TMA. 3-Thiophene acetic acid (3TAA) (98.0%) was purchased from Fluka (Poland). Iron chloride anhydrous (97.0%), dry methanol (99.5%), chloroform (99.9%), and tetrahydrofuran (THF) stabilized with 300 ppm of BHT-PRS (99.5%) were purchased from Panreac Quimica S.A.U. (Spain) and used as received. TPU 12K85 with aromatic grade (ρ = 1.20 g/cm^3), which is a standard polyester-based TPU that combines hardness with excellent mechanical properties, was kindly supplied by Merquinsa (Spain). The chemical structure of the components of this TPU corresponds to a copolymer sequence that involves two aromatic diisocyanates and two aliphatic diols, specifically, 1,4-butanediol and a macrodiol based on poly(butylene adipate), which affords the degradable ester linkages. P3TMA was prepared by a two-step chemical oxidative polymerization using 3TAA as starting monomer. Details about the synthetic process were reported in previous works.[29,34] The yield of P3TMA was ca. 61% after removing the residual oxidant and oligomers.

Molecular weights were estimated by size exclusion chromatography using a liquid chromatograph (Shimadzu, model LC-8A) equipped with an Empower computer program (Waters). A PL HFIP gel column (Polymer Lab) and a refractive index detector (Shimadzu RID-10A) were employed. P3TMA was dissolved and eluted in hexafluoroisopropanol at a flow rate of 0.5 mL/min (injected volume 100 μL, sample concentration 1.5 mg/mL) and using poly(methyl methacrylate) standards. The resulting number and weight-average molecular weights were $\bar{M}_n$ = 24365 g·mol^{-1} and $\bar{M}_w$ = 36524 g·mol^{-1}, respectively. The doping level was obtained from reduction of approximately 2 mg of polymer with carbon, followed by determination of the amount of chloride released by standard ion chromatography. This analysis was performed with a Kontron 600 HPLC liquid chromatograph fitted with a Waters IC-Pak anion column at 30 °C and equipped with a Wescan conductometric detector. This analysis revealed that each repeat unit of P3MTA contains 0.27 counterions (one positive charge per ∼3.7 repeat units). Accordingly, as-synthesized P3TMA contains 6.0 wt % ± 0.29 wt % of Cl^- counterions or 26.2 wt % ± 0.99 wt % of $FeCl_4^-$ counterions.

Lipase F-AP15 (from *Rhizopus oryzae*) was purchased from Sigma (U.S.A.) and used in the enzymatic degradation experiments. For cell culture experiments, Vero and Cos-7 cells were purchased from ATCC (U.S.A.). Dulbecco's phosphate buffered saline solution (PBS) without calcium chloride and magnesium chloride, Dulbecco's modified Eagle's medium (DMEM, with 4500 mg of glucose/L, 110 mg of sodium pyruvate/L, and (2 mM) L-glutamine), penicillin-streptomycin, 3-(4,5-dimethylthiazol-2-yl)-2,5-diphenyltetrazolium bromide (MTT, 97.5%), and trypsin-EDTA solution (0.05% trypsin, 0.02% EDTA) were all purchased from Sigma-Aldrich (USA). Fetal bovine serum (FBS) and trypan blue stain (0.4%) were purchased from Gibco, U.K. Dimethyl sulfoxide (99.0%) was purchased from Panreac Quimica S.A.U. (Spain) and sodium azide (NaN3, ≥99.5%) from Sigma-Aldrich (U.S.A.).

For the protein adsorption assessment, collagen solution Type I from calf skin (0.1% solution in 0.1 M acetic acid) and Lowry reagent were purchased from Sigma-Aldrich.

Preparation of Blends. In order to obtain 5 mg/mL (0.5 wt %) solutions, the given amounts of neat TPU and P3TMA powder were separately dissolved in THF. P3TMA was sonicated for 10 min before (powder) and after its dissolution. After this, the solution was filtered with cotton as a separation barrier. In contrast, TPU was dried at 120 °C under vacuum for 2 h prior to its dissolution. The resulting TPU:P3TMA mixtures, which were prepared considering three different weight ratios (20:80, 40:60, and 60:40), were subsequently stirred at room temperature for 2 h. The dispersions were then filtered and used for film deposition.

Preparation of Nanomembranes. The procedure used for the fabrication of supported and free-standing TPU:P3TMA nano-

membranes was recently described and, therefore, in this work has been only summarized.[34] Supported nanomembranes were obtained by spin-coating at 4000 rpm for 60 s directly onto the substrate (ITO, glass or steel). The thickness of the resulting nanomembranes was found to be 40−50 nm.[34] Although blends were processed as supported nanomembranes for most of the experiments, it should be noted that blends were also processed as films by solvent-casting because of experimental limitations in some of the tests conducted.

FTIR Spectroscopy. IR absorption spectra were recorded on a FTIR Jasco 4100 spectrophotometer. Samples were placed in an attenuated total reflection accessory (Top-plate) with a diamond crystal (Specac model MKII Golden Gate Heated Single Reflection Diamond ATR). TPU and TPU:P3TMA films were solvent casted from the corresponding THF solutions, while P3TMA was analyzed as powder. For each sample 32 scans were performed between 4000 and 600 cm^{-1} with a resolution of 4 cm^{-1}.

Atomic Force Microscopy (AFM). The surface morphology and topography of TPU, P3TMA, and TPU:P3TMA nanomembranes supported on ITO were studied by AFM (image window 5.0 × 5.0 μm^2) using a silicon TAP 150-G probe (Budget Sensors, Bulgaria) with a frequency of 150 kHz and a force constant of 5 N/m. Images were obtained with an AFM Multimode (Veeco) using a NanoScope controller under ambient conditions, in tapping mode. The row scanning frequency was set at 1 Hz. The root mean square roughness (RMS Rq), which is the average height deviation taken from the mean data plane, was determined using the statistical application of the NanoScope Analysis software (1.20, Veeco).

AFM was also conducted to obtain topographic information about the type I collagen structures developed on the samples surface (see below). A silicon probe was used (resonant frequency and spring constant of 200−400 kHz and 40 N/m, respectively). All images were obtained in tapping mode with an AFM Dimension 3100 microscope and a NanoScope IV controller under ambient conditions.

Cyclic Voltammetry (CV). Electrochemical behavior of TPU, P3TMA, and TPU:P3TMA nanomembranes supported on steel AISI 316 was determined by cyclic voltammetry (CV). Measurements were carried out using acetonitrile with 0.1 M $LiClO_4$ and phosphate buffer saline (PBS, pH = 7.4) with 0.1 M $LiClO_4$ as electrolytic solutions, hereafter denoted Acn+$LiClO_4$ and PBS+$LiClO_4$, respectively. All electrochemical experiments were performed with a Potentiostat Versastat II connected to a PC and controlled through the Electrochemistry Power Suite 2.58 (Princeton Applied Research) program using a three-electrode cell under a nitrogen atmosphere (99.995% in purity) at room temperature. The working compartment was filled with 50 μL of the electrolyte solution. Steel AISI 316 sheets of 1 cm^2 were used as both the working and the counter electrodes, and an Ag|AgCl electrode was used as the reference electrode which contained a KCl saturated aqueous solution (offset potential versus the standard hydrogen electrode, E^0 = 0.222 V at 25 °C). All potentials given in this report are referenced to this electrode. Cyclic voltammograms were registered at a scan rate of 20, 50, and 100 mV/s in the potential range from −0.4 to +1.0 V.

The electroactivity, which indicates the ability to store charge, was evaluated by examining the similarity between the anodic and cathodic areas of the control voltammogram. The electrochemical stability (i.e., loss of electroactivity, LEA), which decreases with the oxidation and reduction areas of consecutive control voltammograms, was determined using the following expression:

$$\mathrm{LEA} = \frac{\Delta Q}{Q_i} 100 \tag{1}$$

where ΔQ is the difference of voltammetric charge between the second cycle and the last cycle and Q_i is the voltammetric charge corresponding to the first cycle. In this work all values of LEA were referenced to 10 consecutive oxidation−reduction cycles.

Thermal Degradation. TPU and TPU:P3TMA films were solvent casted from THF solutions onto Teflon sheets and slowly dried under vacuum for 3 days. P3TMA was analyzed as powder. Thermal degradation was determined at heating rates of 5, 10, 20, 30, and 40 °C/min with around 5 mg samples in a Q50 thermogravimetric analyzer of TA Instruments under a flow of dry nitrogen and in the temperature range from 50 to 600 °C. Activation energies were determined by the Kissinger method[36] and the advanced isoconversional method provided by Kissinger−Akahira−Sunose (KAS).[36,37]

According to the nonisothermal kinetics theory, thermal degradation of a sample can be expressed by the following function:

$$\frac{d\alpha}{dT} = \frac{1}{\beta} A e^{(-E/RT)} f(\alpha) \tag{2}$$

where β is the heating rate, T is the absolute temperature, R is the gas constant, $f(\alpha)$ is the differential conversion function, and A and E are the pre-exponential factor and the activation energy for the decomposition reaction step, respectively.

The Kissinger method gives the activation energy at the maximum of the derivative thermogravimetric curve (DTG) for each degradation step. The analysis is based on the following equation:

$$\ln \frac{\beta}{T_{max}^2} = \ln \frac{AR}{E} + \ln[n(1-\alpha_{max})^{n-1}] - \frac{E}{RT_{max}} \tag{3}$$

where T_{max} is the temperature at the maximum reaction rate, α_{max} is the conversion at this T_{max} temperature, n is the reaction order, and A is the frequency factor. From a plot of ln β/T_{max}^2 versus $1/T_{max}$, the activation energy of the degradation step can be determined.

The activation energy during the whole degradation process can be calculated by the KAS method. This methodology is based on eq 2, which after reordering gives

$$\ln \frac{\beta}{T^2} = \ln\left[\frac{AR}{g(\alpha)E}\right] - \frac{E}{RT} \tag{4}$$

where $g(\alpha)$ is the integral conversion function (i.e., $g(\alpha) = \int_0^\alpha d\alpha/f(\alpha)$).

For each degree of conversion and each step of the degradation process the activation energy is obtained from the linear representation of ln β/T^2 versus $1/T$.

Uptake of Water. For the swelling experiments, TPU and TPU:P3TMA films were cast from THF solutions onto Teflon sheets and slowly dried under vacuum for 3 days. The resulting films were easily separated from the Teflon sheets and cut into 1 cm × 1 cm pieces. The thickness, which was assessed by profilometry, was ∼3 μm in the inner region and ∼6 μm on the edges. P3TMA films could not be prepared due to poor film forming characteristics.

Swelling was evaluated by recording the weight increase of the samples placed in vessels filled with 5 mL of PBS solution at 37 °C (four samples for each system). Vessels were closed and sealed with parafilm to prevent water loss by evaporation. Measurements were run over 6 days. At each immersion time, samples were taken out from the oven, carefully dried with delicate task wipers in order to remove water from the surface, and finally weighed on an analytical balance. The percentage of water uptake (WU) was obtained by the ratio between the weight of the samples before and after immersion:

$$\mathrm{WU}\ (\%) = \frac{m_W - m_D}{m_D} \times 100 \tag{5}$$

where m_D is the dried sample mass and m_W the wet sample mass.

Hydrolytic and Enzymatic Degradation. Degradation studies were carried out on TPU and TPU:P3TMA films prepared by solvent casting onto Teflon sheets and cut to approximately 1 cm × 1 cm. Films were placed in vials containing 10 mL of phosphate buffered saline solution (PBS) supplemented with 0.1 mg/mL of sodium azide—to prevent contamination—with and without 4 mg/mL of Lipase F-AP15 to evaluate enzymatic and hydrolytic degradation, respectively. Incubation at 37 °C in a shaking incubator set at 100 rpm lasted for a total of 12 weeks. Vials were closed and sealed with parafilm to avoid loss of solution by evaporation, even though the PBS solution was replaced every 48 h. Samples were analyzed after 1, 2, 4, 6, 8, 10, and 12 weeks.

After each immersion time, samples were removed from the solution and gently washed with distillated water. After drying under vacuum for several days at room temperature, films were weighed. Degradation was quantitatively monitored as weight loss (WL, in %) of the films by applying the following formula:

$$\mathrm{WL} = \frac{m_0 - m_t}{m_0} \times 100 \quad (6)$$

where m_0 is the weight of the film before the degradation assay and m_t is the weight of the film after exposure to the degradation medium.

Cellular Adhesion and Viability. All cellular assays were performed using Vero and Cos-7 cells, which are epithelial- and fibroblast-like, respectively, from monkey kidney. These carcinogenic cells were selected because they can be cultured easily in the presence of serum. Cells were cultured in DMEM high glucose supplemented with 10% FBS, penicillin (100 units/mL), and streptomycin (100 μg/mL). The cultures were maintained in a humidified incubator with an atmosphere of 5% CO_2 and 95% O_2 at 37 °C. Culture media were changed every 2 days. When the cells reached 80−90% confluence, they were detached using 1−2 mL of trypsin (0.25% trypsin/EDTA) for 5 min at 37 °C. Finally, cells were resuspended in 5 mL of fresh medium, and their concentration was determined by counting with a Neubauer camera using 0.4% trypan blue as a vital dye.

TPU, P3TMA, and TPU:P3TMA (20:80, 40:60, and 60:40 compositions) nanomembranes were prepared by spin-coating on steel AISI 316 pieces of 1 cm^2 and then placing in plates of 24 wells and sterilizing using UV light for 15 min in a laminar flux cabinet. Controls were simultaneously performed by culturing cells on the surface of the tissue culture polystyrene (TCP) plates and steel plates. For adhesion assays, an aliquot of 50 μL containing 5×10^4 cells was deposited on the nanomembrane of each well. Then, cell attachment to the nanomembrane surface was promoted by incubating under culture conditions for 30 min. Finally, 500 μL of the culture medium were added to each well. After 24 h, nonattached cells were washed out while attached cells were quantified. For viability assays, the 50 μL aliquots deposited on each well contained 2×10^4 cells. Quantification of viable cells was performed after 7 days of culture.

Cell adhesion and viability were evaluated by the colorimetric MTT [3-(4,5-dimethylthiazol-2-yl)-2,5-diphenyltetrazolium bromide] assay, which determines the cell viability.[38] This assay measures the ability of the mitochondrial dehydrogenase enzyme of viable cells to cleave the tetrazolium rings of the MTT and form formazan crystals, which are impermeable to cell membranes and, therefore, are accumulated in healthy cells. This process is detected by a color change: the characteristic pale yellow of MTT transforms into the dark-blue of formazan crystals. Specifically, 50 mL of MTT solution (5 mg/mL in PBS) was added to each well. After 3 h of incubation, samples were washed twice with PBS and stored in clean wells. In order to dissolve formazan crystals, 1 mL of DMSO/methanol/water (70/20/10% v/v) was added. Finally, the absorbance at 540 mm was measured using a UV−vis spectrophotomether (UV-3600, Shimadzu). The resulting viability results were normalized to TCP control as relative percentages. Results were derived from the average of four replicates ($n = 4$) for each independent experiment.

Type I Collagen Adsorption: Sample Preparation and Quantitative Test. ITO (0.5 × 1.0 cm^2) and glass (square pieces of 1.3 cm^2 area) supported nanomembranes were incubated with collagen type I following the next procedure, which is based on the producer recommendations. A water drop (100 μL) was deposited onto the substrate to hydrate its surface and allow uniform protein dispersion. Then, 10 μL of as-received 1 g/L type I collagen weak acid solution was added. Collagen adsorption was allowed to take place during 1 h at room temperature. After, 400 μL of water were added to prevent evaporation during the prolonged incubation step, and nanomembranes were incubated in the collagen solution overnight at room temperature. Then, the samples were thoroughly washed with distilled water to remove collagen not adsorbed. Type I collagen adsorption was quantitatively determined by the Lowry microassay. Samples were prepared in triplicate.

Type I collagen solution was used as-received (in 0.1 M acetic acid solution): 10 μL of as-received 1 g/L type I collagen weak acid solution was added to 100 μL of water (which had been added before onto each nanomembrane to hydrate its surface and allow uniform protein dispersion afterward), thus diluting the solution 10-fold as recommended by the producer (0.1 g/L) in situ on the nanomembrane surface. The low concentration collagen solution was not used directly because by following our procedure we could hydrate the nanomembrane surface before the protein binding step and expect to get more uniform collagen dispersion throughout the sample.

Contact Angle. Contact angle measurements were obtained using the water drop method. Images of 0.4 μL distillated water drops on the nanomembrane surfaces were recorded after stabilization with the equipment OCA 15EC (DataPhysics Instruments GmbH, Filderstadt), six times for each sample. The software SCA20 was used to analyze the images and acquire the contact angle value.

Statistical Analyses. ANOVA and Tukey tests were performed to determine the statistical significance of contact angle, cell viability, and collagen adsorption results. A confidence level of 95% ($p < 0.05$) was considered.

Scanning Electron Microscopy (SEM). Cells and collagen fibrils adsorption were observed using a Focused Ion Beam Zeiss Neon40 scanning electron microscope equipped with an energy dispersive X-ray (EDX) spectroscopy system and operating at 5 kV. All samples were previously coated with a carbon layer of 6−10 nm thickness using a K950X Turbo Evaporator to prevent sample charging problems. Before the carbon coating, samples covered with cells were fixed in a 2.5% glutaraldehyde PBS solution (pH = 7.2) overnight at 4 °C. Then, they were dehydrated by washing in an alcohol battery (30°; 50°; 70°; 90°; 95°; and 100°) at 4 °C for 30 min per wash. Finally, samples were air-dried and sputter-coated with carbon.

RESULTS AND DISCUSSION

Structural, Morphological, Topographical, and Electrochemical Characterization. Before assessing properties associated with the potential biomedical application of the TPU:P3TMA system, a more general characterization was conducted. Concretely, it included the assessment of the chemical structure of the samples, the evaluation of the nanomembranes surface topology both from a qualitative and quantitative approach, and finally the determination of their electrochemical response. Samples of 20:80, 40:60, and 60:40 TPU:P3TMA composition were studied, to correlate the characterization results with the sample composition.

Figure 1 shows the FTIR spectra of P3TMA, TPU, and TPU:P3TMA blends in the range from 1800 to 900 cm^{-1}.

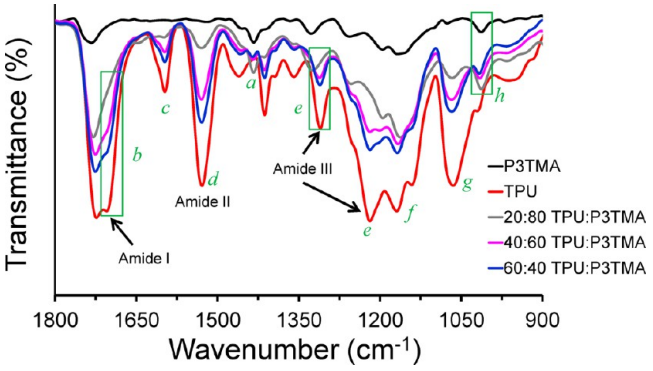

Figure 1. FTIR spectrum of P3TMA, TPU, and 20:80, 40:60, and 60:40 TPU:P3TMA blends in the range 1800−900 cm^{-1}. Absorption bands are described in Table 1. Changes in the peaks marked with labels *a*−*h* (in green) have been used to identify the formation of blends.

Table 1. Main Infrared Absorption Bands (cm^{-1}) of TPU, P3TMA, and 20:80, 40:60, and 60:40 TPU:P3TMA Blends (labels are identified in Figure 1)

			TPU:P3TMA			
absorption bands		P3TMA	20:80	40:60	60:40	TPU
CH_3 bending	*a*	1431	1430	1433	1435	
C═O ester	*b*	1730	1726	1723, 1704	1723, 1703	1724, 1704
C═C stretching phenyl ring (HS)	*c*		1593	1595	1595	1595
N—H bending C—N stretching	*d*		1526	1527	1527	1526
C—N stretching	*e*		1319[a]	1308,1215	1308, 1215	1308, 1215
C—O—C stretching	*f, g*		1164, 1067	1166, 1138, 1067	1168, 1142, 1067	1166[b], 1138, 1062

[a]Shifted by conjugated diene C═C (1325 cm^{-1}). [b]Band overlapped with C—O—C groups from P3TMA.

Results evidence the formation of TPU:P3TMA blends by the overlapping of absorption bands coming from the two individual polymers, TPU and P3TMA. The bands observed for the P3TMA are fully consistent with those reported in our previous work,[30] and, therefore, their description has been omitted. As it is reported in Table 1, the presence of P3TMA in the blends is confirmed by the $-CH_3$ bending absorption at 1431 cm^{-1} (peak *a* in Figure 1) and the changes and shifts occurring at region *e*. Moreover, another band arising from the P3TMA contribution is observed between 1008 and 1017 cm^{-1} for the three composition blends (peak *h*).

The rest of peaks marked (from *b* to *g*) correspond to TPU groups present in the blends. First, the hydrogen bonded C═O stretching band coming from urethane carbonyl groups appears as a small shoulder in the blends spectra at 1701 cm^{-1} (peak *b*) in the C═O stretching band associated with the soft segment ester groups (1719 cm^{-1}, amide I region). Second, transmittance peaks observed at 1595 cm^{-1} (peak *c*) and 1526 cm^{-1} (peak *d*) are consistent with the TPU C═C stretching of the phenyl ring and the C—N stretching + N—H bending (amide II band), respectively. Other bands arising from TPU hard-segment groups (C—N stretching, amide III region) are identified at 1215 cm^{-1} (strong absorption) and 1308 cm^{-1} (weaker absorption). However, those bands are clearly detected only for 60:40 and 40:60 TPU:P3TMA compositions. Finally, the absorption bands seen in the blends at 1166 and 1138 cm^{-1} (peaks *f*) are attributed to the C—O—C stretching of TPU soft segments, while the peak observed at 1061 cm^{-1} (peak *g*) correspond to the C—O—C stretching of both TPU soft and hard segments. Overall, the position and intensity of the absorption bands in TPU:P3TMA blends spectra are in good agreement with their composition.

AFM images of P3TMA, TPU, and 20:80, 40:60 and 60:40 TPU:P3TMA supported nanomembranes onto ITO and prepared by spin-coating are displayed in Figure 2. We examined the influence of the composition on the morphology and topography of the samples surface. In addition to the characterization of the two individual polymers and the 40:60 TPU:P3TMA nanomembrane, which were exhaustively discussed in our previous work,[35] here the 60:40 and 20:80 compositions are also analyzed. As it can be seen, the characteristics of the 40:60 and 60:40 TPU:P3TMA samples consist of irregular distributions of relatively prominent and well-defined folds, the RMS roughness being very similar for the two compositions (i.e., 20 and 19 nm for 60:40 and 40:60 TPU:P3TMA, respectively). Therefore, both compositions are found in an intermediate position between TPU and P3TMA since the morphology of TPU consists of a smooth surface with multiple and well-localized folds homogeneously distributed (RMS roughness of only 6 nm), whereas the surface of P3TMA

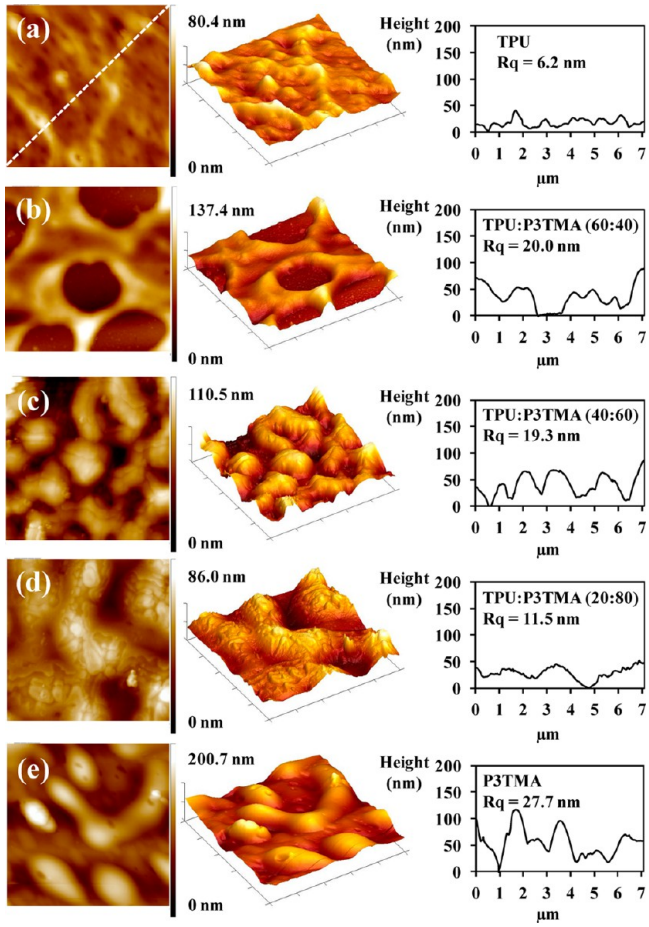

Figure 2. AFM topographic images of the ITO-supported nanomembranes: (a) TPU, (b) 60:40 TPU:P3TMA, (c) 40:60 TPU:P3TMA, (d) 20:80 TPU:P3TMA, and (e) P3TMA. 2D height images (left column), 3D height images (middle column), and cross-section profiles (right column) from the diagonal line for each sample as depicted in (a). RMS Rq values are also provided. In all cases the image window is 5.0 × 5.0 μm^2.

is significantly more irregular (RMS roughness of 28 nm). Finally, the irregular surface of 20:80 TPU:P3TMA is more similar to that of P3TMA, even though the RMS roughness (12 nm) is closer to that of TPU.

The electrochemical response of the 20:80, 40:60, and 60:40 TPU:P3TMA nanomembranes supported on steel was studied in different electrolytic media by cyclic voltammetry (CV) and compared with that obtained for individual P3TMA and TPU. Supporting Information Figure S1a shows the first control voltammograms recorded in Acn+$LiClO_4$ while those obtained

dx.doi.org/10.1021/am502150q | ACS Appl. Mater. Interfaces 2014, 6, 9719−9732

after 10 consecutive oxidation−reduction cycles in the same environment are displayed in Figure 3a. The first control

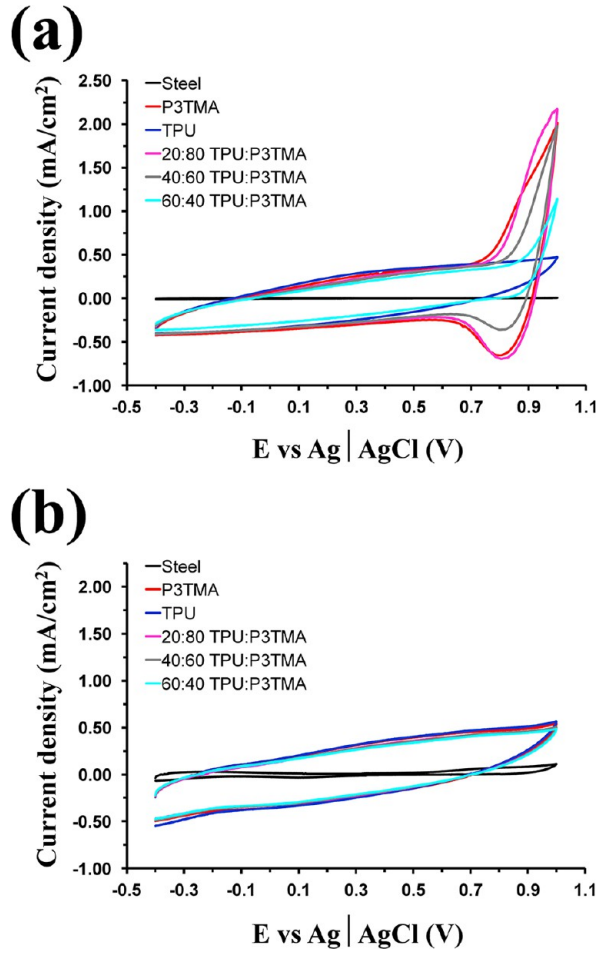

Figure 3. Voltammogram after 10 consecutive oxidation−reduction cycles for P3TMA, TPU, 20:80 TPU:P3TMA, 40:60 TPU:P3TMA, 60:40 TPU:P3TMA, and uncoated steel in (a) Acn+$LiClO_4$ and (b) PBS+$LiClO_4$. Scan rate: 20 mV/s. Initial and final potential: −0.4 V; reversal potential: 1.0 V.

voltammogram of P3TMA shows an oxidation peak and a shoulder at 0.80 and 0.93 V, respectively, which indicate the formation of polarons and bipolarons. After 10 redox cycles they shift to lower potentials (0.77 and 0.87 V, respectively), and the shoulder becomes more pronounced. These two oxidation processes as well as the reduction of polarons and bipolarons, which are both detected at a potential of 0.76 V for P3TMA, are clearly identified in the three TPU:P3TMA compositions. Moreover, voltammograms indicate that the electroactivity decreases with the concentration of P3TMA for the three TPU:P3TMA compositions. However, the influence of P3TMA is very remarkable in all cases, as the electroactivity of the 20:80, 40:60, and 60:40 TPU:P3TMA nanomembranes is lower than that of individual P3TMA by only 9%, 15%, and 24%, respectively. After 10 oxidation−reduction cycles, the 20:80, 40:60, and 60:40 TPU:P3TMA nanomembranes show similar LEA values (38%, 31%, and 35%, respectively), lower than that for P3TMA, which is 48% after 10 cycles. In opposition, TPU does not show well-defined oxidation or reduction processes in Acn+$LiClO_4$. However, comparison of the voltammograms recorded for bare steel and TPU indicates that the former substrate is completely inactive from an electrochemical point of view within the scanned interval of potentials, whereas the latter shows some electrochemical activity. Thus, the voltammograms recorded for TPU are consistent with the formation of charged species at unspecific positions, representing a significant difference with respect to P3TMA in which polarons and bipolarons are formed at preferred positions. Inspection of the anodic and cathodic areas indicates that the electroactivity of TPU is 65% lower than that of P3TMA in the first control voltammogram, this value decreasing to 58% after 10 redox cycles. These results indicate that the formation of charged species in TPU through oxidation and reduction processes does not occur at the preferred position, as is observed for P3TMA.

Voltammograms recorded in PBS+$LiClO_4$ for the investigated systems are displayed in Supporting Information Figures S1b and 3b. The large similarity between the anodic and cathodic areas in the first voltammogram recorded for P3TMA, which shows weak oxidation and reduction shoulders at 0.86 and 0.09 V, respectively, indicates that the ability to store charge is 30% higher in PBS+$LiClO_4$ than in Acn+$LiClO_4$. Moreover, the LEA is only 23% after 10 redox cycles in PBS +$LiClO_4$, about half of the value observed in Acn+$LiClO_4$. Similarly, the electrochemical stability of the TPU:P3TMA nanomembranes is significantly high as is evidenced by the estimated LEA values: 21%, 24%, and 23% for the 20:80, 40:60, and 60:40 compositions, respectively. Thus, the LEA for the blends is around 15% lower in PBS+$LiClO_4$ than in Acn +$LiClO_4$. Finally, the first voltammogram of TPU in PBS +$LiClO_4$ is similar to that recorded for P3TMA, which explains that the electroactivity of the former material is only 2% lower than that of the latter. Interestingly, the LEA of TPU is about 12% after 10 cycles, evidencing that the electrostability of this material is higher than that of P3TMA.

Thermal Properties. Partial miscibility of TPU:P3TMA samples has recently been demonstrated from calorimetric studies.[34] The glass transition temperatures (T_g) of these blends were always observed at temperatures intermediate between those characteristic of the two polymers (i.e., −10 and 62 °C for TPU and P3TMA, respectively). For example, the 50:50 TPU:P3TMA sample has two T_g values at −1 and 56 °C, indicative of the formation of two amorphous phases with different compositions. All studied samples were amorphous withthe exception of pure TPU, which exhibited a relatively low melting temperature in the 124−131 °C range depending on the processing conditions (e.g., solvent casting and spin coating).[34] According to possible applications of new blends, it seems also highly interesting to evaluate their thermal stability and the degradation processes.

Thermogravimetric scans (Supporting Information Figure S2) show that all P3TMA-containing samples started to decompose at a relatively low temperature (ca. 140 °C), 10% degradation requiring a temperature higher than 280 °C (i.e., far away from the melting temperature). Decomposition of blends was characterized by two main degradation steps as shown in the derivative thermogravimetric (DTG) curves (Figure 4a) for the 50:50 TPU:P3TMA representative sample. These steps are related with a low temperature degradation process, most probably due to the initiation of the P3TMA degradation, and a high temperature degradation process that could be associated mainly with decomposition of TPU.

The DTG curves of TPU and P3TMA samples (Figure 4a) reveal highly complex degradation processes with at least three

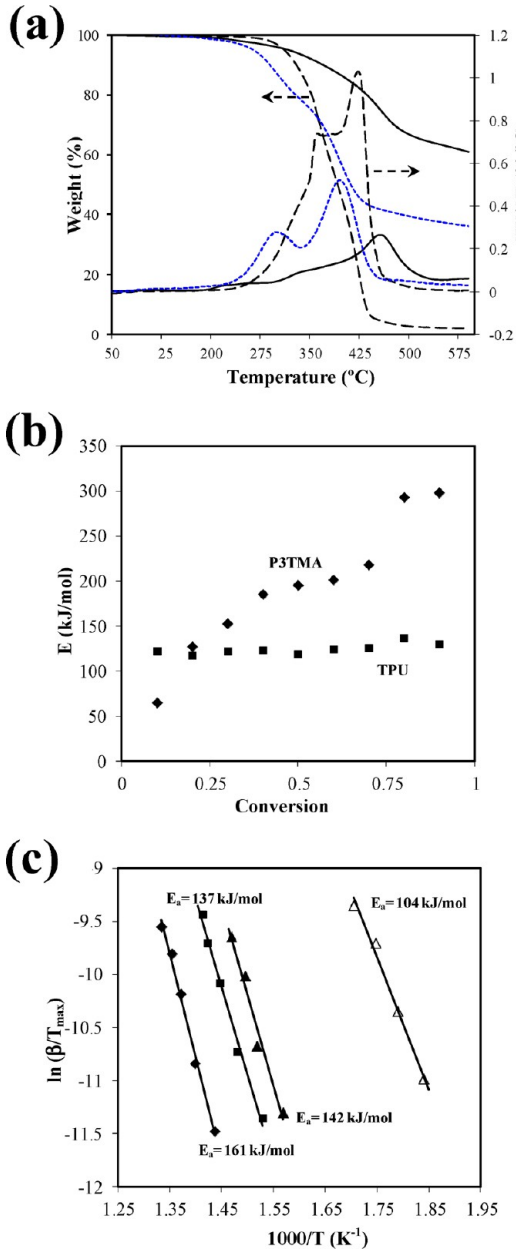

Figure 4. (a) Thermogravimetric and derivative thermogravimetric curves corresponding to the thermal decomposition of TPU (black and dashed lines), P3TMA (black and solid lines), and 50:50 TPU:P3TMA (blue and dotted lines). (b) Plots of the activation energy calculated by the KAS method as a function of the conversion degree for TPU (■) and P3TMA (◆) homopolymers. (c) Kissinger plots for the main decomposition step of the TPU (■) and P3TMA (◆) homopolymers, and the two degradation steps of the 50:50 TPU:P3TMA blend (▲, Δ). Full and empty symbols correspond to the peaks appearing at the higher and lower temperature, respectively.

steps. The main decomposition process occurred at the highest temperature for both polymers (i.e., 430 and 460 °C for TPU and P3TMA, respectively) and involved practically a 50% of the relative weight loss and gave rise to well-defined DTG peaks. Despite the complex decomposition process of TPU, its activation energy remained practically constant (ca. 124 kJ/mol) during degradation, as was revealed by the KAS isoconversional analysis (Figure 4b). On the contrary, a high variation was detected for P3TMA (i.e., from 65 to 298 kJ/mol; Figure 4b) as expected for well-differentiated degradation mechanisms.

Kissinger analysis became useful to discern the degradation processes of the polymer blends, although it can be considered a rough approximation since it is not a rigorous isoconversional method. As shown in Figure 4c, activation energies of 104 and 142 kJ/mol were obtained for the two degradation steps detected for the 50:50 TPU:P3TMA sample. The first step occurs, as explained before, at the temperature range where decomposition of P3TMA starts and the associated energy is in agreement with the low values determined for P3TMA at low conversions. The activation energy deduced from the second DTG peak of the blend (i.e., 142 kJ/mol) is in full agreement with the energy derived from the main peak of TPU (137 kJ/mol) and clearly deviates from the higher value (161 kJ/mol) obtained for P3TMA. In addition, it is also clear that thermal degradation of the blend is practically finished at a temperature lower than that associated with the main decomposition step of P3TMA (Figure 4a). In summary, thermal degradation of the blends is determined by the low energy processes associated with each individual polymer, namely, P3TMA at the beginning and TPU at the end.

Swelling. Generally, transfer processes can occur at the material−tissue interface when materials contact biological systems. For instance, fluid can move into the biomaterial device thus leading to an increase of volume, a process known as swelling. The study of this phenomenon is of high importance since water is the most important and primary driver for biointeractions, and the scaffold water absorption capacity is crucial in cell regeneration applications. Besides, swelling can affect profoundly the behavior of the biomaterial, causing large and continual deformations and deterioration of its mechanical properties. Therefore, the water uptake test has been used to evaluate the TPU:P3TMA films swelling properties from a quantitative point of view, special attention being paid to the influence of the composition.

Figure 5 displays the variation of the water uptake values against the immersion time for TPU and TPU:P3TMA solvent-casted films. Films with the higher content of P3TMA, that is, 20:80 and 40:60 TPU:P3TMA, displayed a swelling rate that

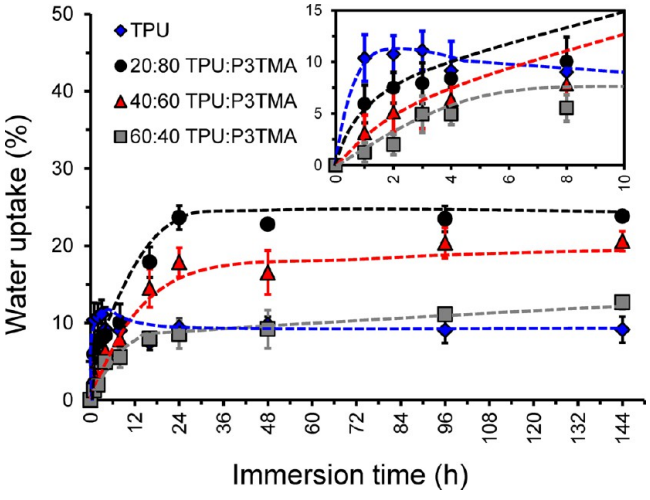

Figure 5. Variation of the water uptake (in %) against the immersion time (in hours) for TPU and TPU:P3TMA films. Inset shows the swelling during the first 10 h of immersion. Dashed lines were added manually to help follow data progression.

dx.doi.org/10.1021/am502150q | ACS Appl. Mater. Interfaces 2014, 6, 9719−9732

increased almost linearly for the first 24 h, reaching values that are slightly constant for the rest of the swelling period, i.e., 24 ± 2% and 18 ± 2%, respectively. During the first 24 h, the water uptake curve for 60:40 TPU:P3TMA films rises up to a swelling ratio of 9 ± 2%, and from that point onward, the water uptake occurs at a much slower pace. It is important to remark that the speed at which the saturation is reached depends mostly on the thickness of the sample, the kinetics of diffusion, and the temperature. Interestingly, TPU films show the highest swelling ratio during the first 3 h, with a maximum at 11 ± 2%. However, the value decreases to 7 ± 1% after 16 h and remains practically constant and similar to the water uptake displayed by 60:40 TPU:P3TMA films.

A linear relationship between the water uptake value and the immersion time is linked to the diffusion of water in the amorphous zones of the polymer. As calorimetric results evidenced, all TPU:P3TMA blends samples exhibited the formation of two amorphous phases with different compositions. Therefore, TPU:P3TMA swelling curves are in good agreement with this observation. In addition to that, water molecules penetrate to void spaces left at the boundaries of the phases.

TPU films undertake severe water absorption at the earlier stages of the swelling process, which induces rupture of intramolecular hydrogen bonds, leading to relaxation movements within TPU polymeric chains. Before reaching the final equilibrium plateau, these movements result in a structural rearrangement of the polymeric chains during a transition step in which water can be ejected.

It can be noted that for all samples the equilibrium plateau is well established after 36 h. In general, swelling increases with P3TMA content. Indeed, at the end of the swelling period, water absorption is approximately twice for 40:60 and 20:80 TPU:P3TMA (21 ± 1% and 24 ± 1%, respectively) than for TPU and 60:40 TPU:P3TMA (9 ± 2% and 13 ± 1%, respectively). These results suggest that, in general, the swelling ability of TPU:P3TMA blends is suitable for their use as biomaterials. Accordingly, the three investigated compositions show a water uptake ability that is expected to affect favorably cellular regeneration through the formation of biointeractions in which water plays a crucial role. Furthermore, measured water absorption capacities indicate that the all blends will undergo hydrolytic degradation, even though this is expected to be higher for the 20:80 and 40:60 blends than for the 60:40 and pure TPU compositions (as has been corroborated in the next section). The process of swelling and its mechanism are decisive to design biomaterial devices with a proper subsequent degradation which relies on the molecular processes involved, that is, penetration of water molecules to void spaces and relaxation of the polymeric matrix segments. By tailoring the TPU:P3TMA composition, several degradation rates can be expected according to the water uptake ratio.

Hydrolytic and Enzymatic Degradation. Effective mimicking of the extracellular matrix (ECM) requires conducting polymer-based tissue scaffolds to be both biodegradable and biocompatible to minimize the inflammatory reaction in a tissue that hosts the biomaterial device. TPU:P3TMA films have been subjected to degradation processes, which can provoke scissions at the backbone of the polymer chains, to assess their suitability for clinical applications as tissue scaffolds.

Figure 6a represents the temporal evolution of the weight loss (WL) measured for TPU and TPU:P3TMA films during

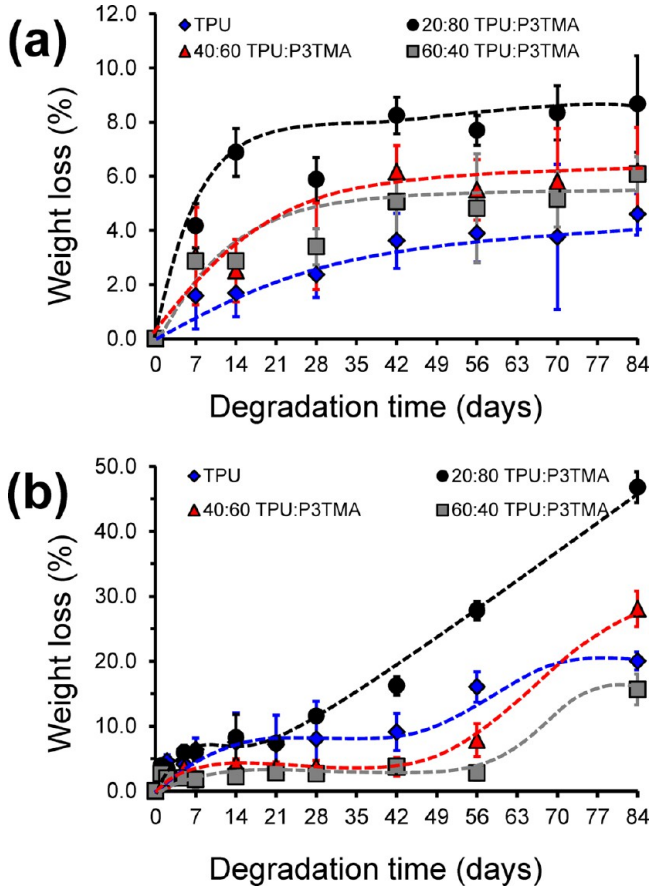

Figure 6. Weight loss of pure TPU and TPU:P3TMA films immersed in (a) PBS solution and (b) lipase-containing PBS solution. Dashed lines were added manually to help following data progression.

12 weeks of immersion in PBS solution. The hydrolytic degradation of TPU:P3TMA samples proceeds at a higher rate than that of TPU samples and depends on the P3TMA content. Thus, degradation of the 20:80 blend, which exhibits WL = 9 ± 2% after 12 weeks of immersion in PBS, occurs significantly faster than that of the 40:60 and 60:40 films, both with a WL= 6 ± 1% after 12 weeks. This behavior is fully consistent with the water uptake results discussed in the previous subsection (Figure 5) and should be attributed to the relatively low partial miscibility between TPU and P3TMA.

On the contrary, the weight of TPU films decreases slowly during the first 6 weeks of immersion, remaining practically unaltered at WL ≈ 4% after such a period of time. The hydrolytic stability of TPU indicates that penetration of water into films is very limited and the weight loss displayed in Figure 6a corresponds to the first stages of surface degradation rather than to the bulk degradation processes. Moreover, the hydrolytic resistance shown by the commercial TPU used in this work is fully consistent with that recently observed for other thermoplastic polyurethanes tuned by incorporating higher concentration of biodegradable soft segments.[39,40] Thus, the hydrolytic degradation of TPU is known to take place through the hydrolysis of the ester groups of the polyester soft segment.[41] Figure 6b displays the temporal evolution of the weight loss measured for TPU and TPU:P3TMA films during 12 weeks of immersion in the Lipase-containing solution. As it can be seen, the enzyme clearly enhances significantly the

degradation process for all the compositions. Again, the P3TMA content influences the enzymatic degradation rate.

The 20:80 TPU:P3TMA blend exhibits the higher weight loss during the degradation period, escalating from WL = 8 ± 4% at week 2 to WL = 47 ± 2% after 12 weeks of immersion in PBS solution with Lipase. Interestingly, the weight loss evolution for 20:80 TPU:P3TMA films is similar to that shown by TPU films during the first quarter of the immersion period. However, the blend starts a severe fragmentation process after only 3 weeks, which leads to a dramatic increase in the weight loss value that is ascribed to a critical loss of mechanical properties. Although TPU films also evidence a rising trend, this is much steadier since films are able to retain their mechanical properties. The final WL value for TPU is 20 ± 1% after 12 weeks of immersion.

Within this context, it should be emphasized that 40:60 and 60:40 blends present a similar weight loss behavior during the first half of the immersion period by showing practically equal WL values, even though this is slightly lower than those reported for TPU and 20:80 TPU:P3TMA films. Similarly, at week 6 there is a considerable increase in the weight loss for 40:60 and 60:40 TPU:P3TMA films, which rise from 4 ± 1% each to 28 ± 3% and 16 ± 2%, respectively.

TPU films behavior is consistent with the surface mechanism reported for TPUs when exposed to lipase,[42] typical of enzymatic attack,[43] whereas for TPU:P3TMA films it depends on the amount of P3TMA. Specifically, the presence of P3TMA hinders the degradation processes for 40:60 and 60:40 blends by possibly preventing the access to cleavage points in the TPU molecular chains during the enzymatic attack, until a point is reached at which the loss of mechanical properties prevails. On the other hand, the degradation process is fully controlled by the loss of mechanical features in the case of the 20:80 TPU:P3TMA films.

Therefore, biodegradation results reveal that the TPU matrix is essential to provide mechanical integrity to conducting polymer-based tissue scaffolds, while specific compositions of TPU:P3TMA films behave not only as a semiconductor but also as a biodegradable material.

Biocompatibility. A key factor when developing conducting polymer-based devices to be attractive candidates as tissue scaffolds is their biocompatibility and immunogenity. Bearing that requirement in mind, the biocompatibility of TPU:P3TMA nanomembranes has been assessed by cell adhesion and viability tests. Moreover, the response of 20:80, 40:60, and 60:40 TPU:P3TMA toward Vero and Cos-7 cellular lines has been compared with those of TPU and P3TMA. Two substrates, TCP and steel, were used as control in all adhesion and viability assays.

Quantitative results for cell adhesion assays are displayed in Figure 7a. The number of Vero and Cos-7 cells adhered to the surface of the TPU:P3TMA nanomembranes is higher than that of P3TMA thin films. Indeed, cellular adhesion onto TPU:P3TMA increases with decreasing content of P3TMA. This tendency is more evident in the case of Vero cells. The adhesion of both Vero and Cos-7 on the surface of TPU nanomembranes is the most favored, comparable to the TCP control result, whereas steel shows the worst behavior as supportive matrix for cellular adhesion.

After 7 days of culture, the cellular activity on the materials was re-evaluated. Cellular viability results, which are included in Figure 7b, show an appreciable increment in the cellular colonization for all the TPU:P3TMA compositions. Evaluation

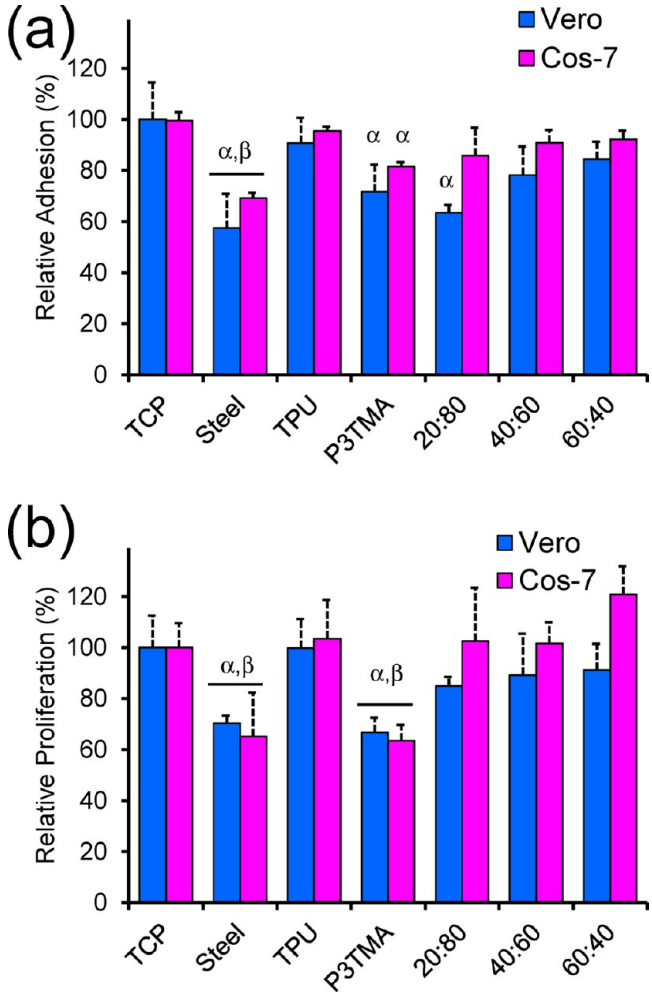

Figure 7. Relative cellular adhesion (a) and viability (b) on TPU, P3TMA, and TPU:P3TMA (20:80, 40:60, and 60:40 ratios) nanomembranes. Assays were carried out using the following cell lines: Vero (blue bars) and Cos-7 (purple bars). The relative viability was established in relation to the TCP control (tissue culture polystyrene). Steel was also considered as a control substrate because the individual polymers and the blends were deposited on this material. Greek letters on the columns refer to significant differences ($p < 0.05$) using the ANOVA and Tukey test: α vs TCPS; β vs steel.

of this increment with respect to the viability of the adhered cells indicates that the preference of Vero and Cos-7 cells is higher for the 20:80 and 60:40 compositions, respectively, even though in absolute terms the biocompatibility exhibited by TPU:P3TMA blends increases with the concentration of TPU. In contrast, P3TMA inhibits cell viability, which may be attributed to the presence of $FeCl_3$ in the polymeric matrix. This oxidizing agent, which is in excess during the polymerization process, has been reported to provoke cytotoxicity in MCF-7 cells[44] and to induce lipid peroxidation in cell membranes.[45] Finally, the viability of Vero and Cos-7 cells in TPU increases slightly while that of steel remains practically unaltered (Cos-7 cells) or increases (Vero cells). In order to corroborate the cytotoxicity of $FeCl_3$, viability assays were performed using TPU films previously immersed in an aqueous solution containing 20 μg/mL $FeCl_3$. Results showed that viability of Vero and Cos-7 cells decreases by 23% ± 3% and 31% ± 6%, respectively, in relation with the values obtained for TPU without $FeCl_3$.

dx.doi.org/10.1021/am502150q | ACS Appl. Mater. Interfaces 2014, 6, 9719−9732

Viability results obtained for TPU:P3TMA blends can be related with the surface structure of the nanomembranes through two key features. The first refers to the roughness, in general cell viability after 24 h and 7 days increasing with the surface roughness. Thus, the formation of connection sites between the cells and the surface of TPU:P3TMA nanomembrane becomes easier for nanomembranes with higher roughness. Second, cell viability increases with the miscibility of the two components in the nanomembranes. Thus, 2D phase AFM images indicate that the partial miscibility is higher for the 40:60 and 40:60 compositions than for the 20:80, which is fully consistent with quantitative results obtained for cell adhesion and viability assays. Overall, TPU:P3TMA can be considered as effective bioactive platform.

SEM micrographs displayed in Figure 8 show the characteristics of Vero cells cultured onto the surface of TPU, P3TMA, and TPU:P3TMA nanomembranes. Inspection of the SEM micrographs for TPU:P3TMA nanomembranes (Figure 8e–j) indicates that the receptivity of the surface to colonization through cellular viability of adhered cells increases with the content of TPU. Although large microdomains without cells are identified on the surface of 20:80 TPU:P3TMA thin films, cells are widely spread on the surface of 40:60 and, especially, 60:40 TPU:P3TMA nanomembranes. In addition, the connection sites between the cells and the surface of TPU:P3TMA are clearly identified in Figure 8h–j. These consist of actin filaments, which are known as fillopodia, oriented toward the film surface for local adhesion. It is worth noting their similarities with the formation of cellular monolayers on the surface of TPU (Figure 8a,b). In general, there is a broad spreading of cells on TPU, even though very small domains without cells are occasionally detected (Figure 8a, inset). In contrast, bare P3TMA frequently shows micrometric surface areas without cells (Figure 8c,d), which is consistent with the relatively low cell viability found for this P3TMA as compared to that of TPU and TPU:P3TMA nanomembranes (Figure 7). Indeed, the biological behavior of P3TMA is considerably worse than that observed for other biocompatible polythiophene derivatives, as, for example, poly(3,4-ethylenedioxythiophene).[46] SEM micrographs of Cos-7 adhered to the surface of the different substrates (not shown) were fully consistent with these trends. In all, these results indicate that TPU:P3TMA nanomembranes are not only biocompatible but also stimulate the cellular viability.

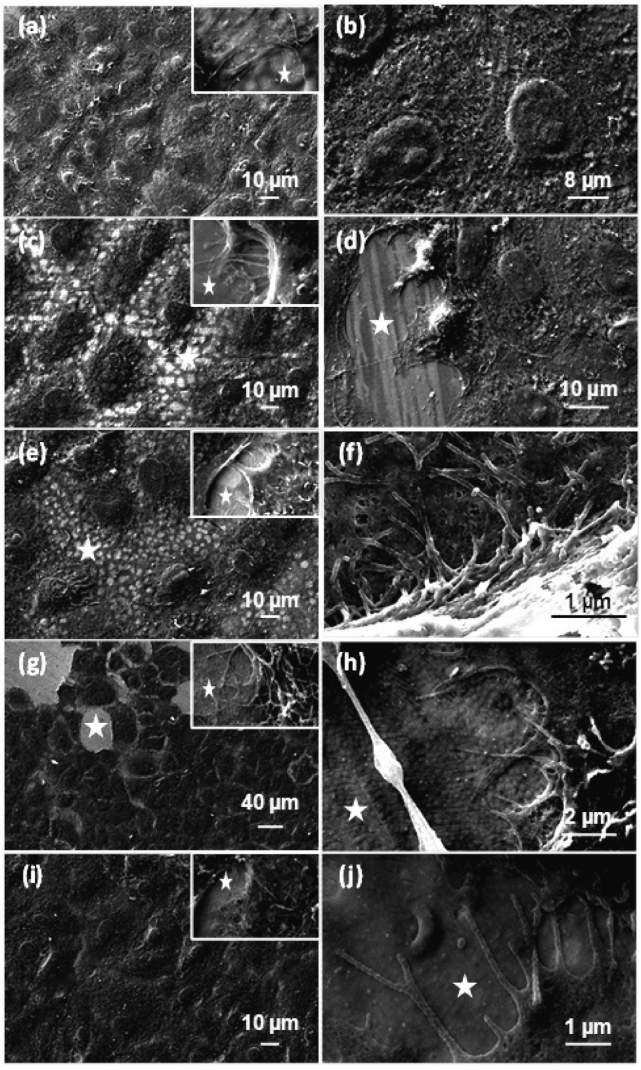

Figure 8. SEM micrographs of Vero cells cultured on the surface of TPU (a and b), P3TMA (c and d), 20:80 TPU:P3TMA (e and f), 40:60 TPU:P3TMA (g and h), and 60:40 TPU:P3TMA (i and j) substrates. Left images show adhesion results (inset: interactions between cells and the substrate surface) and right images show colonization results after 7 days. Surface without cells is indicated with a star (★).

At this stage, a close examination of the results described so far designate the 40:60 TPU:P3TMA composition the most adequate composition for further assays since it achieved a balance between good electrochemical properties and suitable swelling, biodegradation, and biocompatible features. Besides, it presents good mechanical[34] and conducting[35] properties, exhaustively studied at the nanometric scale in previous work. Concretely, the next subsection discusses the behavior of 40:60 TPU:P3TMA nanomembranes as bioactive platforms by analyzing their protein adsorption response.

Type I Collagen Adsorption. Protein adsorption onto surfaces is the first stage that takes place in cell adhesion and viability processes when biomaterials contact living cells in the appropriated media. Type I collagen is the most common collagen isotype. In addition, type I collagen is one of the most abundant extra cellular matrix (ECM) proteins, which is known to bind fibronectin, another important ECM protein, for early adhesion.[47] Various types of interactions may influence the adsorption of collagen, which depend both on the protein and the surface of the sample. Surface properties like wettability, linked to topography, roughness, and chemistry, have been shown to alter protein adsorption and conformation, influencing the cellular response of a material.[48,49]

Quantitative data on collagen type I adsorption onto ITO and glass supported TPU, P3TMA, and 40:60 TPU:P3TMA nanomembranes are displayed in Figure 9. Protein adsorption onto bare ITO, glass coverslips, and TCP were used as control. As depicted in Figure 9, no significant difference on the collagen adsorption (79–81%/cm^2) was obtained regardless of the sample surface when ITO was employed as substrate. Surprisingly, the adsorption of collagen on the bare glass coverslip, which was also used as the control substrate, is 36 ± 2%/cm^2, less than the half of the value obtained for ITO substrate. This value is similar to that obtained for TCP, 29 ± 1%/cm^2 (not included in Figure 9). In order to further understand this difference, contact angle measurements were

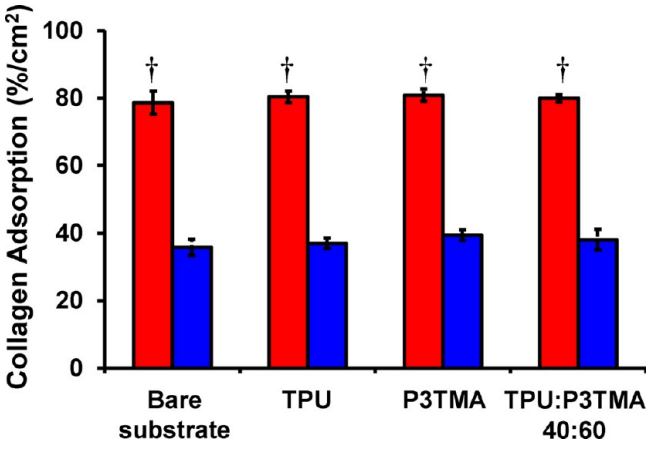

Figure 9. Type I collagen adsorption quantitative data (%/cm^2). Ultrathin nanomembranes spin-coated onto ITO (red bars) and glass coverslips (blue bars). (†) Tukey test, $p < 0.05$ vs respective glass support.

carried out. The contact angles determined for the bare substrates are 75° ± 3° and 68° ± 2° for ITO and glass, respectively, showing a difference of 7°.

Following these observations, the protein adsorption test was repeated for nanomembranes spin-coated onto glass coverslips to determine the influence of the substrate. Again, values of adsorbed collagen showed no significant difference regardless of the nanomebmrane composition but were all almost half the values obtained for ITO-supported nanomembranes (37−39%/cm^2). This behavior could be attributed to the differences in the surface wettability of the different substrates. Contact angle values determined for TPU, P3TMA, and 40:60 TPU:P3TMA nanomembranes spin-coated onto ITO are 81° ± 1°, 82° ± 1°, and 81° ± 2°, respectively; whereas, when spin-coated onto glass, values slightly decrease to 78° ± 2°, 79° ± 2°, and 79° ± 1°, respectively. All these values are higher than the corresponding bare substrate contact angle value, regardless the nanomembrane. Therefore, TPU, P3TMA, and TPU:P3TMA supported nanomembranes exhibit the same degree of wettability when spin-coated onto the same substrate. Once type I collagen was adsorbed onto a glass substrate, the contact angle test was repeated and the value dropped from 68° ± 2° to 36° ± 2°. The same decreasing tendency was observed for the nanomembranes, although in a lower extent for the TPU (69° ± 4°), and in a greater extent for P3TMA and 40:60 TPU:P3TMA (50° ± 2° for both materials). Finally, it is important to highlight that TPU, P3TMA, and 40:60 TPU:P3TMA nanomembranes behave as active surfaces for the adsorption of collagen.

In general, factors that monitor the ECM protein adsorption mechanism, such as the substrate wettability, are not understood completely yet.[50−53] Inspection of the bare substrates (ITO and glass) response indicates that the amount of adsorbed protein decreases with the contact angle value (i.e., hydrophobicity promotes adsorption of collagen type I). Nevertheless, analysis of the TPU, P3TMA, and 40:60 TPU:P3TMA responses evidence that such simple and direct correlation cannot be applied. It becomes evident that other factors apart from wettability can affect the protein adsorption mechanism.

SEM and AFM images were recorded for type I collagen adsorbed onto ITO supported nanomembranes (TPU, P3TMA, and 40:60 TPU:P3TMA) and bare ITO substrate to evaluate the influence of the topography on the adsorbed collagen structures. Type I collagen adsorbed onto 40:60 TPU:P3TMA nanomembranes surface forms at least two layers (Figure 10). More specifically, the top layer exhibits a

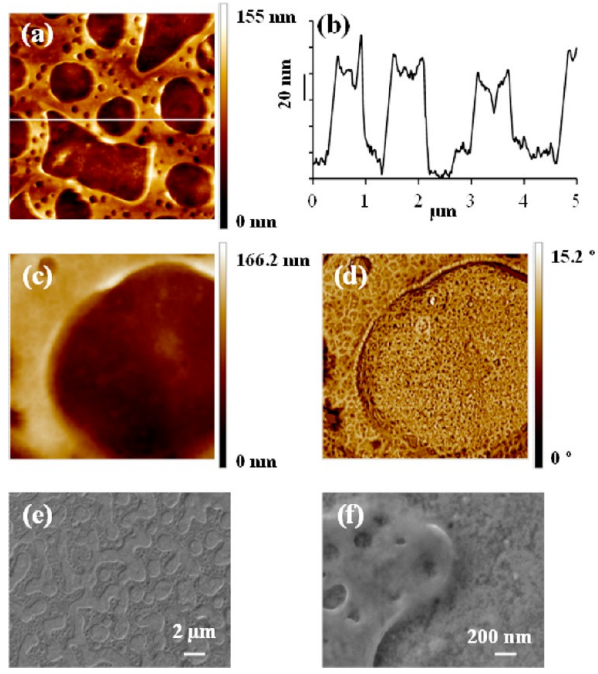

Figure 10. SEM-AFM images of type I collagen adsorbed onto 40:60 TPU:P3TMA nanomembrane: (a) height image 5 × 5 μm^2; (b) cross-sectional data from (a); (c) height image 1 × 1 μm^2; (d) phase image 1 × 1 μm^2 of (c); (e and f) SEM images (14 k× and 150 k×, respectively).

pseudoregular honeycomb 2D network (Figure 10a) that shows cavities with different sizes. The larger pits present diameters of 1.2 ± 0.7 μm, while the smaller ones, whose diameter is 194 ± 55 nm, are uniformly distributed throughout the surface. Besides, cross-section profile data (Figure 10b) indicate depths of about 73 nm. A careful inspection of a smaller area of the surface (Figure 10c,d) reveals a fibril structure on the top layer. The bottom layer is similar to the top one although collagen adopts a much more compact configuration.

Type I collagen topography adsorbed onto 40:60 TPU:P3TMA nanomembranes shares some similarities with that adsorbed on TPU and P3TMA nanomembranes surfaces (Figures 11 and 12). Specifically, it also adopts a two layer arrangement. However, type I collagen adsorbed onto TPU results in a matrix with a regular distribution of pits on the top layer (Figure 11a1,a2), whereas the bottom layer is more uniform and adsorbed collagen is closely packed together (Figure 11a3,a4). Cross-section profile data show that the depth of such pits ranges from 5 to 8 nm (Figure 12a2). On the contrary, for the P3TMA nanomembrane, the collagen adsorbed top layer is more dense and with smaller cavities, which display height steps of 46.4 nm in some regions and diameters of 227 ± 46 nm and are distributed throughout the surface (Figure 11b1,b2). Moreover, the fibrous collagen matrix on the top layer (Figure 11b3,b4) resembles that for 40:60 TPU:P3TMA, while the bottom layer is comparable in all three samples, regardless of the nanomembrane composition.

dx.doi.org/10.1021/am502150q | ACS Appl. Mater. Interfaces 2014, 6, 9719−9732

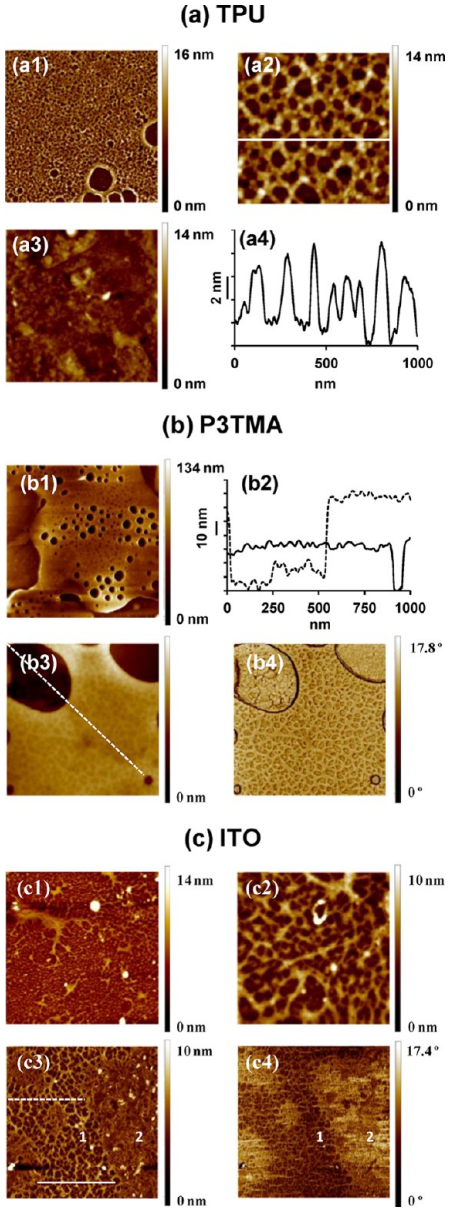

Figure 11. AFM images of type I collagen adsorbed onto (a) TPU and (b) P3TMA nanomembranes and (c) bare ITO. For TPU: (a1) height image 5 × 5 μm^2; (a2) height image 1 × 1 μm^2; (a3) height image 1 × 1 μm^2; and (a4) cross-sectional data from (a2). For P3TMA: (b1) height image 5 × 5 μm^2; (b2) cross-sectional data from (b3); (b3) height image 1 × 1 μm^2; and (b4) phase image 1 × 1 μm^2 of (b3). For bare ITO: (c1) height image 5 × 5 μm^2; (c2) height image 1 × 1 μm^2; (c3) height image 3 × 3 μm^2; and (c4) phase image 3 × 3 μm^2 of (c3).

Finally, Figures 11c and 12c displays images for type I collagen deposited onto bare ITO. In this case, type I collagen topography differs from the one observed for the TPU:P3TMA supported nanomembranes. Particularly, fibrils appear to be arranged on branching structures and the collagen matrix does not cover the entire surface since ITO substrate is detected (dark regions in phase image of Figure 11c2). Moreover, these fibrils result in a porous collagen matrix with several high density regions, in which collagen shows a more compacted structure and fibrils are not distinguished. Cross-section profiles reveal that the diameter and height of the fibrils varied from 40 to 140 nm and from 1 to 4 nm, respectively.

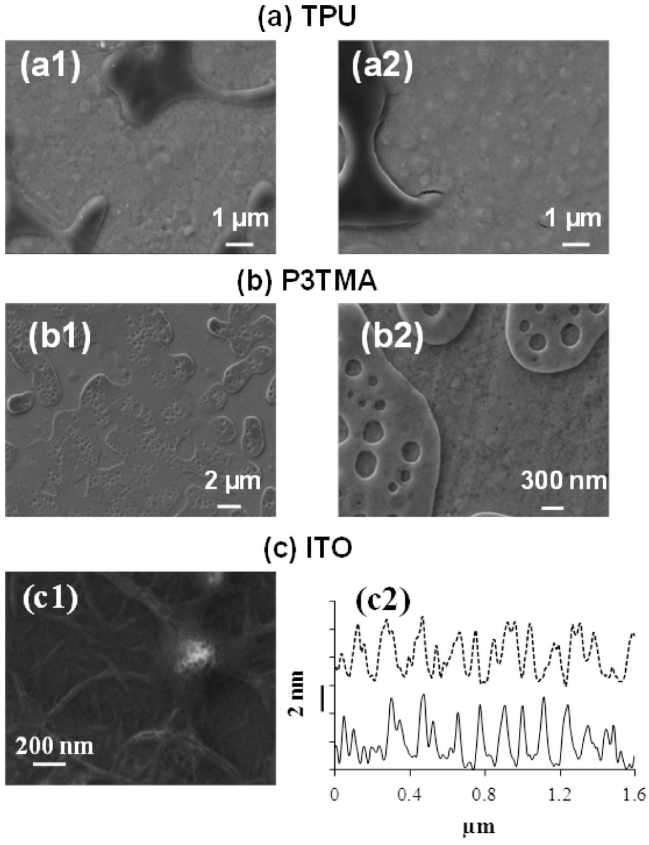

Figure 12. SEM images of type I collagen adsorbed onto (a) TPU and (b) P3TMA nanomembranes and (c) bare ITO. For TPU: (a1) and (a2) images at 30 k×. For P3TMA: images at (b1) 14 k× and (b2) 80 k×. For bare ITO: (c1) image at 152 k× and (c2) cross-sectional data from Figure 11c3.

Finally, SEM images allowed us to identify the type I collagen fibrous structures adsorbed onto the several surfaces. Results are in good agreement with the previous AFM observations.

As a general consideration, morphological observations by SEM and AFM showed that the sample surface affects the adsorbed type I collagen structure and distribution. Type I collagen adsorbed onto the nanomembranes hides the original surface by entirely covering it. The final adsorption topography varies slightly depending on the nanomembrane film, which may be influenced by both the chemical composition and also the roughness of the nanomembranes.[54] In general terms, collagen matrix presents a 2D honeycomb-like morphology when adsorbed onto TPU, P3TMA, and 40:60 TPU:P3TMA nanomembranes, in opposition to the results obtained for the bare ITO substrate. As it has been stated elsewhere,[55,56] honeycombed collagen matrixes are suitable scaffolds for biological and biomedical purposes.

CONCLUSIONS

The influence of the composition of the properties, especially those oriented toward biomedical applications, of TPU:P3TMA nanomembranes has been examined. The topography and morphology displayed by these systems is intermediate between those of the two individual components. Thus, the 40:60 and 60:40 samples consist of irregular distributions of prominent and well-localized folds while 20:80 nanomembranes show an irregular surface that resembles that of P3TMA. The electrochemical response of the blends and individual

dx.doi.org/10.1021/am502150q | ACS Appl. Mater. Interfaces 2014, 6, 9719−9732

polymers is similar in PBS, while in acetonitrile the ability to store charge and the electrostability of TPU:P3TMA nanomembranes increases and decreases, respectively, with the content of P3TMA.

The water uptake observed for TPU:P3TMA films decreases with the concentration of TPU, even though it is relatively high in all cases. Consistently, hydrolytic and enzymatic degradation increase with the P3TMA content. This behavior should be attributed to the phase separation between TPU and P3TMA regions, which facilitates the access of water molecules to the bulk. The response of TPU:P3TMA to lipase-containing PBS solutions is that expected from biodegradable materials. Furthermore, viability assays show that TPU:P3TMA are biocompatible blends, the viability of cells increasing with the concentration of TPU in the composition.

Studies on type I collagen reveal that the amount of adsorbed protein does not depend on the chemical composition of the organic nanomembranes but on the substrate used as support. However, the surface that contacts the protein affects the morphology of adsorbed collagen matrices. Collagen onto bare ITO form fibrils while honeycomb-like structures are observed when the protein is in contact with organic nanomembranes, the dimensions and regularity of such organization being dependent on the chemical nature of the nanomembrane.

The behavior of TPU:P3TMA nanomembranes, especially the 40:60, as electroactive substrates for biomedical applications is very good. Thus, these hydrophilic blend nanomembranes are biodegradable and promote cell growth. In addition, adsorption of collagen results in the formation of honeycomb protein matrices with potential applications as three-dimensional scaffolds for tissue engineering. Current research is oriented toward cell regeneration onto 40:60 TPU:P3TMA bioactive substrates through electrical stimulation for different advanced biomedical applications.

■ ASSOCIATED CONTENT

Ⓢ Supporting Information

First control voltammograms and thermogravimetric curves for P3TMA, TPU, and TPU:P3TMA blends. This material is available free of charge via the Internet at http://pubs.acs.org.

■ AUTHOR INFORMATION

Corresponding Authors

*E-mail: fsanz@ub.edu (F.S.).
*E-mail: carlos.aleman@upc.edu (C.A.).

Notes

The authors declare no competing financial interest.

■ ACKNOWLEDGMENTS

Financial support from the MINECO and FEDER (MAT2012-34498 and MAT2012-36205), Generalitat de Catalunya (2009SGR925, 2009SGR277, 2009SGR1208, and XRQTC) and CIBER-BBN is gratefully acknowledged. CIBER-BBN is an inititiative funded by the VI National R&D&I Plan 2008-10211, Iniciativa Ingenio 2010, Consolider Program, CIBER Actions, and financed by the Instituto de Salud Carlos III with assistance from the European Regional Development Fund. Support for the research of C.A. was received through the prize "ICREA Academia" for excellence in research funded by the Generalitat de Catalunya. M.M.P.-M. is grateful for financial support through a FPI-UPC grant.

■ REFERENCES

(1) Wallace, G. G.; Higgins, M. J.; Moulton, S. E.; Wang, C. Nanobionics: the Impact of Nanotechnology on Implantable Medical Bionic Devices. *Nanoscale* **2012**, *4*, 4327−4347.

(2) Guimard, N. K.; Gomez, N.; Schmidt, C. E. Conducting Polymers in Biomedical Engineering. *Prog. Polym. Sci.* **2007**, *32*, 876−921.

(3) Kim, D.-H.; Wiler, J. A.; Anderson, D. J.; Kipke, D. R.; Martin, D. C. Conducting Polymers on Hydrogel-Coated Neural Electrode Provide Sensitive Neural Recordings in Auditory Cortex. *Acta Biomater.* **2010**, *6*, 57−62.

(4) Svennersten, K.; Berggren, M.; Richter-Dahlforsa, A.; Jager, E.W. H. Mechanical Stimulation of Epithelial Cells Using Polypyrrole Microactuators. *Lab Chip* **2011**, *11*, 3287−3293.

(5) Abidian, M. R.; Kim, D. H.; Martin, D. C. Conducting-Polymer Nanotubes for Controlled Drug Release. *Adv. Mater.* **2006**, *18*, 405−409.

(6) Bendrea, A.-D.; Cianga, L.; Cianga, I. Progress in the Field of Conducting Polymers for Tissue Engineering Applications. *J. Biomater. Appl.* **2011**, *26*, 3−84.

(7) Hardy, J. G.; Lee, J. Y.; Schmidt, C. E. Biomimetic Conducting Polymer-Based Tissue Scaffolds. *Curr. Opin. Biotechnol.* **2013**, *24*, 847−962.

(8) Jun, I.; Jeong, S.; Shin, H. The Stimulation of Myoblast Differentiation by Electrically Conductive Sub-Micron Fibers. *Biomaterials* **2009**, *30*, 2038−2047.

(9) Kim, Y. D.; Kim, J. H. Synthesis of Polypyrrole-Polycaprolactone Composites by Emulsion Polymerization and the Electrorheological Behavior of Their Suspensions. *Colloid Polym. Sci.* **2008**, *286*, 631−637.

(10) Guo, B.; Finne-Wistrand, A.; Albertsson, A. C. Facile Synthesis of Degradable and Electrically Conductive Polysaccharide Hydrogels. *Biomacromolecules* **2011**, *12*, 2601−2609.

(11) Guiseppi-Elie, A. Electroconductive Hydrogels: Synthesis, Characterization and Biomedical Applications. *Biomaterials* **2010**, *31*, 2701−2716.

(12) Mire, C. A.; Agrawal, A.; Wallace, G. G.; Calvert, P.; in het Panhuis, M. Inkjet and Extrusion Printing of Conducting Poly(3,4-ethylenedioxythiophene) Tracks on and Embedded in Biopolymer Materials. *J. Mater. Chem.* **2011**, *21*, 2671−2678.

(13) Ku, S. H.; Lee, S. H.; Park, C. B. Synergic Effects of Nanofiber Alignment and Electroactivity on Myoblast Differentiation. *Biomaterials* **2012**, *33*, 6098−6104.

(14) Greco, F.; Zucca, A.; Taccola, S.; Menciassi, A.; Fujie, T.; Haniuda, H.; Takeoka, S.; Dario, P.; Mattoli, V. Ultra-Thin Conductive Free-Standing PEDOT/PSS Nanofilms. *Soft Matter* **2011**, *7*, 10642−10650.

(15) Matovic, J.; Jaksic, Z.; Grober, P.; Bruckner, D.; Hellmich, C.; Schmiedmayer, H. B.; Stachelberger, H.; Gebehuber, I. C. Bionic (Nano)Membranes. *Biomimetic − Material, Structures and Processes*; Springer-Verlag: Berlin, 2011.

(16) Lee, C.; Wei, X. D.; Kysar, J. W.; Hone, J. Measurement of the Elastic Properties and Intrinsic Strength of Monolayer Graphene. *Science* **2008**, *321*, 385−388.

(17) Kim, K. S.; Zhao, Y.; Jang, H.; Lee, S. Y.; Kim, J. M.; Kim, K. S.; Ahn, J. H.; Kim, P.; Choi, J. Y.; Hong, B. H. Large-Scale Pattern Growth of Graphene Films for Stretchable Transparent Electrodes. *Nature* **2009**, *457*, 706−710.

(18) Mueggenburg, K. E.; Lin, X. M.; Goldsmith, R. H.; Jaeger, H. M. Elastic Membranes of Close-Packed Nanoparticle Arrays. *Nat. Mater.* **2007**, *6*, 656−660.

(19) Rogers, J. A.; Lagally, M. G.; Nuzzo, R. G. Synthesis, Assembly and Applications of Semiconductor Nanomembranes. *Nature* **2011**, *477*, 45−53.

(20) Striemer, C. C.; Gaborski, T. R.; McGrath, J. L.; Fauchet, P. M. Charge- and Size-Based Separation of Macromolecules Using Ultrathin Silicon Membranes. *Nature* **2007**, *445*, 749−753.

(21) Vendamme, R.; Onoue, A.; Nakao, A.; Kunitake, T. Robust Free-Standing Nanomembranes of Organic/Inorganic Interpenetrating Networks. *Nat. Mater.* **2006**, *5*, 494−501.
(22) Watanabe, H.; Muto, T.; Ohzono, T.; Nakao, A.; Kunitake, T. Giant Nanomembrane of Covalently-Hybridized Epoxy Resin and Silica. *J. Mater. Chem.* **2009**, *19*, 2425−2431.
(23) Watanabe, H.; Ohzono, T.; Kunitake, T. Fabrication of Large, Robust Nanomembranes from Diverse, Cross-Linked Polymeric Materials. *Macromolecules* **2007**, *40*, 1369−1371.
(24) Watanabe, H.; Kunitake, T. A Large, Freestanding, 20 nm Thick Nanomembrane Based on an Epoxy Resin. *Adv. Mater.* **2007**, *19*, 909−912.
(25) Watanabe, H.; Ohzono, T.; Kunitake, T. Fabrication of Large Nanomembranes by Radical Polymerization of Multifunctional Acrylate Monomers. *Polym. J.* **2008**, *40*, 379−382.
(26) Fujie, T.; Matsutani, N.; Kinoshita, M.; Okamura, Y.; Saito, A.; Takeoka, S. Adhesive, Flexible, and Robust Polysaccharide Nanosheets Integrated for Tissue-Defect Repair. *Adv. Funct. Mater.* **2009**, *19*, 2560−2568.
(27) Toshinori, F.; Yosuke, O.; Shinji, T. Ubiquitous Transference of a Free-Standing Polysaccharide Nanosheet with the Development of a Nano-Adhesive Plaster. *Adv. Mater.* **2007**, *19*, 3549−3553.
(28) Okamura, Y.; Kabata, K.; Kinoshita, M.; Saitoh, D.; Takeoka, S. Free-Standing Biodegradable Poly(lactic acid) Nanosheet for Sealing Operations in Surgery. *Adv. Mater.* **2009**, *21*, 4388−4392.
(29) Armelin, E.; Gomes, A. L.; Pérez-Madrigal, M. M.; Puiggalí, J.; Franco, L.; del Valle, L. J.; Rodíguez-Galán, A.; Campos, J. S. C.; Ferrer-Anglada, N.; Alemán, C. Biodegradable Free-Standing Nanomembranes of Conducting Polymer:Polyester Blends as Bioactive Platforms for Tissue Engineering. *J. Mater. Chem.* **2012**, *22*, 585−594.
(30) Pérez-Madrigal, M. M.; Armelin, E.; del Valle, L. J.; Estrany, F.; Alemán, C. Bioactive and Electroactive Response of Flexible Polythiophene:Polyester Nanomembranes for Tissue Engineering. *Polym. Chem.* **2012**, *3*, 979−991.
(31) Kang, E.; Ryoo, J.; Jeong, G. S.; Choi, Y. Y.; Jeong, S. M.; Ju, J.; Chung, S.; Takayama, S.; Lee, S.-H. Large-Scale, Ultrapliable, and Free-Standing Nanomembranes. *Adv. Mater.* **2013**, *25*, 2167−2173.
(32) Beebe, D. J.; Mensing, G. A.; Walker, G. M. Physics and Application of Microfluidics in Biology. *Annu. Rev. Biomed. Eng.* **2002**, *4*, 261−286.
(33) Liu, W. F.; Chen, C. S. Engineering Biomaterials to Control Cell Function. *Mater. Today* **2005**, *8*, 28−35.
(34) Pérez-Madrigal, M. M.; Giannotti, M. I.; Oncins, G.; Franco, L.; Armelin, E.; Puiggali, J.; Sanz, F.; del Valle, L. J.; Alemán, C. Bioactive Nanomembranes of Semiconductor Polythiophene and Thermoplastic Polyurethane: Thermal, Nanostructural and Nanomechanical Properties. *Polym. Chem.* **2013**, *4*, 568−583.
(35) Pérez-Madrigal, M. M.; Giannotti, M. I.; Armelin, E.; Sanz, F.; Alemán, C. Electronic, Electric and Electrochemical Properties of Bioactive Nanomembranes Made of Polythiophene: Thermoplastic Polyurethane. *Polym. Chem.* **2014**, *5*, 1248−1257.
(36) Kissinger, H. E. Reaction Kinetics in Differential Thermal Analysis. *Anal. Chem.* **1957**, *29*, 1702−1706.
(37) Akahira, T.; Sunose, T. Method of Determining Activation Deterioration Constant of Electrical Insulating Materials. *Res. Report Chiba Inst. Technol.* **1971**, *16*, 22−31.
(38) Mosmann, T. Rapid Colorimetric Assay for Cellular Growth and Survival: Application to Proliferation and Cytotoxicity Assays. *J. Immunol. Methods* **1983**, *65*, 55−63.
(39) Zukiene, K.; Jankauskaite, V.; Betingyte, V.; Baltuanikas, A. Properties of Recycled Polycaprolactone−Based Thermoplastic Polyurethane Filled with Montmorillonites. *J. Appl. Polym. Sci.* **2013**, *128*, 2186−2196.
(40) Lluch, C.; Lligadas, G.; Ronda, J. C.; Galia, M.; Cádiz, V. Thermoplastic Polyurethanes From Undecylenic Acid-Based Soft Segments: Structural Features and Release Properties. *Macromol. Biosci.* **2013**, *13*, 614−622.
(41) Bosworth, L. A.; Downes, S. Physicochemical Characterisation of Degrading Polycaprolactone Scaffolds. *Polym. Degrad. Stab.* **2010**, *95*, 2269−2276.
(42) Gu, X. G.; Wu, J.; Mather, P. T. Polyhedral Oligomeric Silsesquioxane (POSS) Suppresses Enzymatic Degradation of PCL-Based Polyurethanes. *Biomacromolecules* **2011**, *12*, 3066−3077.
(43) Christenson, E. M.; Patel, S.; Anderson, J. M.; Hiltner, A. Enzymatic Degradation of Poly(ether urethane) and Poly(carbonate urethane) by Cholesterol Esterase. *Biomaterials* **2006**, *27*, 3920−3926.
(44) Laqué-Rupérez, E.; Ruiz-Gómez, M. J.; de la Peña, L.; Gil, L.; Martínez-Morillo, M. Methotrexate Ctotoxicity on MCF-7 Breast Cancer Cells is not Altered by Exposure to 25 Hz, 1.5 mT Magnetic Field and Iron (III) Chloride Hexahydrate. *Bioelectrochemistry* **2003**, *60*, 81−86.
(45) Woollard, K. J.; Sturgeon, S.; Chin-Dusting, J. P. F.; Salem, H. H.; Jackson, S. P. Erythrocyte Hemolysis and Hemoglobin Oxidation Promote Ferric Chloride-induced Vascular Injury. *J. Biol. Chem.* **2009**, *284*, 13110−13118.
(46) Fabregat, G.; Ballano, G.; Armelin, E.; del Valle, L. J.; Cativiela, C.; Alemán, C. An Electroactive and Biologically Responsive Hybrid Conjugate Based on Chemical Similarity. *Polym. Chem.* **2013**, *4*, 1412−1424.
(47) Tjia, J. S.; Aneskievich, B. J.; Moghe, P. V. Substrate-Adsorbed Collagen and Cell Secreted Fibronectin Concertedly Induce Cell Migration on Poly(lactide−glycolide) Substrates. *Biomaterials* **1999**, *20*, 2223−2233.
(48) Coelho, N. M.; González-García, C.; Salmerón-Sánchez, M.; Altankov, G. Arrangement of Type IV Collagen on NH_2 and COOH Functionalized Surfaces. *Biotechnol. Bioeng.* **2011**, *108*, 3009−3018.
(49) Coelho, N. M.; Salmeron-Sanchez, M.; Altankov, G. Fibroblast Remodeling of Type IV Collagen at Biomaterials Interface. *Biomater. Sci.* **2013**, *1*, 494−502.
(50) Gurdak, E.; Rouxhet, P. G.; Dupont-Gillain, C. C. Factors and Mechanisms Determining the Formation of Fibrillar Collagen Structures in Adsorbed Phases. *Colloids Surf., B* **2006**, *52*, 76−88.
(51) Liang, Z.; Zhou, C.; Zeng, R.; Cai, H.; Guo, Z. Visualization of the Nanoscale Assembly of Type I Collagen on PLA by AFM. *Scanning* **2010**, *32*, 104−111.
(52) Gurdak, E.; Booth, J.; Roberts, C. J.; Rouxhet, P. G.; Dupont-Gillain, C. C. Influence of Collagen Denaturation on the Nanoscale Organization of Adsorbed Layers. *J. Colloid Interface Sci.* **2006**, *302*, 475−484.
(53) Gurdak, E.; Dupont-Gillain, C. C.; Booth, J.; Roberts, C. J.; Rouxhet, P. G. Nanoscale Organization of Collagen and Mixed Collagen−Pluronic Adsorbed Layers. *Langmuir* **2005**, *21*, 10684−10692.
(54) Woodcock, S. E.; Johnson, W. C.; Chen, Z. Collagen Adsorption and Structure on Polymer Surfaces Observed by Atomic Force Microscopy. *J. Colloid Interface Sci.* **2005**, *292*, 99−107.
(55) George, J.; Onodera, J.; Miyata, T. Biodegradable Honeycomb Collagen Scaffold for Dermal Tissue Engineering. *J. Biomed. Mater. Res., Part A* **2008**, *87*, 1103−1111.
(56) George, J.; Kuboki, Y.; Miyata, T. Differentiation of Mesenchymal Stem Cells into Osteoblasts on Honeycomb Collagen Scaffolds. *Biotechnol. Bioeng.* **2006**, *95*, 404−411.